Research Article

Received: 10 July 2017 Revised: 29 August 2017 Accepted article published: 3 October 2017 Published online in Wiley Online Library:

(wileyonlinelibrary.com) DOI 10.1002/jctb.5462

Hydrogenolysis of glycerol to 1,2-propanediol in a continuous flow trickle bed reactor

Debora L Manuale,[a] Lucía V Santiago,[b] Gerardo C Torres,[a] Jorge H Sepúlveda,[a] Pablo A Torresi,[a] Carlos R Vera[a]* and Juan C Yori[a]

Abstract

BACKGROUND: Hydrogenolysis of glycerol to glycols in continuous flow three phase reactors is of practical importance due to the need to give value to huge amounts of surplus glycerol. Thermodynamic and kinetic aspects must be revised for a proper design. The system was studied in a trickle-bed reactor using copper chromite and Cu/Al_2O_3 as catalysts.

RESULTS: Phase equilibrium and flow pattern were verified. Solid, liquid and gas phases were present, with the liquid phase in 'trickling' flow. Catalysts were characterized by inductively coupled plasma (ICP), nitrogen sortometry, X-ray photoelectron spectroscopy (XPS), X-ray diffraction (XRD), temperature programmed reduction (TPR) and pyridine thermal programmed desorption (TPD). The average reaction rate was found to be practically constant under different process conditions. A theoretical analysis indicated that the resistance to the transfer of hydrogen from the gas to the liquid phase dominated the overall kinetics. Selectivity to 1,2-propanediol varied with temperature, with a maximum at 230 °C (97%). Selectivity was a function of the catalyst acidity. When the pressure was increased the selectivity to 1,2-propanediol was increased, up to 97% at 14 bar. Higher pressures did not modify this value.

CONCLUSIONS: Optimum reaction conditions for maximum selectivity to 1,2-propanediol with Cu-based catalysts are 230 °C and 14 bar. System kinetics are, however, dominated by the gas–liquid mass transfer resistance.

Keywords: catalyst characterization; catalytic reactors; hydrogenation/hydrogenolysis; mass transfer

INTRODUCTION

The rapid development of biodiesel production by transesterification of vegetable oils or animal fats with methanol or ethanol has yielded large amounts of glycerol (Gly) as a by-product.[1] The influx of biodiesel-derived Gly into the commodity Gly market has led to a rapid decline in the Gly price, which has in turn increased the production cost of biodiesel. Therefore, conversion of Gly into high value-added chemicals has become highly desirable because not only does it help to improve the economy of the biodiesel industry but also because it decreases the environmental impact caused by large amounts of Gly being disposed of as waste.[2,3]

Among the plentiful chemicals derived from Gly, propylene glycol (1,2-propanediol, 1,2-PDO) has attracted much attention from researchers in recent years because of its multiple applications. Uses of 1,2-PDO are in unsaturated polyester resins, functional fluids (antifreeze, de-icing and heat transfer), pharmaceuticals, foods and animal feed, cosmetics, liquid detergents, tobacco humectants, flavors and fragrances, personal care products, paints, agricultural adjuvants and chemical commodities.[4–8]

The catalytic hydrogenolysis of Gly to 1,2-PDO is now being recognized as a green and sustainable process for production of propanediols, compared with the traditional and industrially established petroleum-based route of hydration of propylene oxide.[9] Until now a lot of effort has been devoted to developing an efficient hydrogenolysis process.[4,6,9–11] The reaction of Gly hydrogenolysis is usually supposed to proceed by either the dehydration of Gly to acetol (AOL) over acid sites followed by the hydrogenation of AOL on metal sites to 1,2-PDO.[6,9]

Depending on operating conditions and catalyst, different types of compounds can be obtained from Gly. Sun *et al.* used a fixed bed reactor with a commercial Cu/Al_2O_3 catalyst, mainly obtaining 1,2-PDO[12]. Mota *et al.* studied Ru, Pd, Zn and Cu metal catalysts, obtaining propane as a main product.[13] Liu and Ye obtained lactic acid and 1,2-PDO using a Cu catalyst supported over different oxides.[14]

Representative studies on the dehydration–hydrogenation route were made by Seretis and Tsiakaras.[1,15] They studied Ni/SiO_2-Al_2O_3 and Pt/Al_2O_3 catalysts, obtaining high values of Gly conversion (84%) using the Pt catalyst though with low selectivity to 1,2-PDO (25%). Similar results were obtained by Jiang *et al.* with bimetallic Pd-Ni catalysts.[16] Cu-ZnO-Al_2O_3 catalysts were found to be highly efficient for the catalytic hydrogenolysis of

* *Correspondence to: CR Vera, Instituto de Investigaciones en Catálisis y Petroquímica – INCAPE (UNL-CONICET), Predio CONICET CCT Santa Fe, Dr. Alberto Cassano, Colectora Ruta Nacional N° 168 Km 0, Paraje El Pozo, 3000 Santa Fe, Argentina. Email: cvera@fiq.unl.edu.ar*

a *Instituto de Investigaciones en Catálisis y Petroquímica – INCAPE (UNL-CONICET), Santa Fe, Argentina*

b *Facultad de Ingeniería Química – FIQ (UNL), Santiago del Estero, Santa Fe, Argentina*

Gly.[17] High conversion of Gly and high selectivity to 1,2-PDO were obtained over Cu-substituted hydrocalumite catalysts under proper conditions.[18] All the mentioned research works have focused on catalyst preparation and characterization as well as on the optimization of process variables in order to increase Gly conversion and selectivity to 1,2-PDO. A few reports exist on the hydrogenolysis of glycerol using continuous reactors.[19,20] Most of the published works have been undertaken using discontinuous, batch stirred tank reactors. This makes extrapolation to industrial use difficult, since most industrial applications use high pressure continuous tubular reactors.[1,11,21–27]

The objective of this work was to study the reaction of hydrogenolysis of Gly in a continuous packed bed reactor. According to reaction conditions the system could be biphasic (gas–solid) or triphasic (gas–liquid–solid). If it is triphasic many flow patterns are possible (trickle, mist, slug, etc.). In this sense one aspect to be studied was the flow regime present at the optimal conditions for Gly conversion to 1,2-PDO. Results of activity and selectivity were compared for both commercial and laboratory prepared catalysts. The commercial catalyst was copper chromite[28] while Cu/Al_2O_3 was prepared in the laboratory. Copper chromite was chosen because it is one of the most studied catalysts for hydrogenolysis of glycerol. Copper over alumina was chosen because it is a simple but different catalyst with similar active sites. The idea was to use two sufficiently different catalysts subjected to similar mass transfer resistance.

A thermodynamic study was performed to evaluate all feasible reactions and conditions affecting the thermodynamic yield to different products. Also conditions and variables affecting mass and heat transfer resistances were evaluated. Process variables considered were temperature, hydrogen pressure and spatial velocity (LHSV). Their influence on the activity and selectivity of copper chromite and Cu/Al_2O_3 was investigated.

EXPERIMENTAL

Catalysts

A Cu catalyst supported over alumina (Cu/Al_2O_3) was prepared. A γ-Al_2O_3 Ketjen CK300 support was used (cylinders of 1.5 mm calcined at 500 °C for 4 h, 35–60 mesh). An aqueous solution of $Cu(NO_3)_2{\cdot}3H_2O$ (Anedra, >99.9%) was used to impregnate the support by the incipient wetness technique. The volume and concentration of the impregnating solution were adjusted to get a content of 13% Cu (w/w) on the final catalyst. Impregnation was performed at room temperature for 3 h. After impregnation, the solid was dried for 24 h at 120 °C and then calcined in air at 500 °C for 3 h. Before reaction the catalysts were reduced in flowing hydrogen (105 mL min^{-1}) at 250 °C for 3 h. The prepared catalyst was named CA.

Commercial copper chromite catalyst was supplied by Strem Chemicals (Cat. 29-0410, pellets). This catalyst was referred to as CC. Pellets were ground to a 35-80 mesh fraction.

Characterization

The metal content of the catalysts was determined by ICP (inductively coupled plasma) analysis using OPTIMA 2100 Perkin Elmer equipment.

Nitrogen adsorption experiments for pore size distribution, BET surface area and pore volume measurements were performed in an Autosorb-1 Quantachrome instrument. All samples were pretreated at 200 °C for 90 min under vacuum before the measurement.

The superficial electronic state of the metal was studied by XPS assessment of the Cu $2p_{3/2}$ peak. XPS measurements were made in a Multitech UniSpecs XR-50 unit with a dual Mg/Al X-ray source and a hemisphere analyzer Specs Phoibos 150. The sample was treated at 250 °C *ex situ* in flowing hydrogen for 1 h before the XPS measurement.

X-ray diffractograms of each sample were obtained using a Shimadzu XD-1 instrument with Ni filtered CuKα radiation ($\lambda = 1.5405$ Å) in the $15° < 2\theta < 85°$ range and with a scan rate of 1° min^{-1}. Each sample was ground to a fine powder and reduced in hydrogen flow. After cooling in hydrogen it was immediately put into the equipment chamber for analysis. The Cu crystallite medium size of both catalysts was calculated applying the Debye–Scherrer equation.

TPR studies were performed on fresh samples of the catalysts in a Micromeritics Autochem II analyzer measuring the H_2 consumption with a TCD detector (mV signal) after drying the gases in a water-trap. The heating rate of the cell was 10 °C min^{-1} and the reducing gas mixture was 5% H_2/Ar (50 mL min^{-1}).

The acidity of the catalysts was measured by temperature programmed desorption of pyridine. A description of the equipment and methods used can be found elsewhere.[29]

TEM micrographs were obtained using a JEOL 100 CX II equipment, with an acceleration voltage of 100 kV. Micrographs had a magnification of 270000×.

Catalytic test

Figure 1 shows the reaction system. The reaction was performed in a stainless steel packed bed reactor. The reactor was placed inside an oven of controlled temperature. The catalyst was placed over a quartz wool plug placed in the middle of the reactor (internal diameter, ID = 11 mm). Before reaction the catalyst was reduced *in situ* at 250 °C in hydrogen (AGA, 99.9%) for 1–3 h.

H_2 was fed to the reactor by means of a Cole-Parmer mass flow controller and the system pressure was regulated with a Swagelok backpressure controller. Then an 80 wt% aqueous solution of Gly (Ciccarelli, >99.9%) was fed to the top of the reactor. The solution was previously heated at 70–80 °C in a flask in order to reduce its viscosity. The reaction products leaving the reactor were cooled down in a condenser and the gas and liquid products were separated in a pressurized vessel upstream of the backpressure controller.

The catalytic test was performed using the following conditions: 4 g of catalyst (35–80 mesh), temperature was varied between 210 and 250 °C, H_2 pressure was set in the 8–20 bar range, H_2 flow was set at 48 NmL min^{-1}, and the liquid space velocity (LHSV) was varied between 1.9 and 5.63 h^{-1} (reactant flow rate of 0.15–0.45 mL min^{-1}).

The reaction conditions for both the commercial copper chromite catalyst and the supported copper catalyst were exactly the same.

The reaction products were sampled periodically and analyzed off-line in a Shimadzu 2014 gas chromatograph equipped with a FID detector and a capillary column (30 m × 0.25 mm internal diameter) J&W INNOWax 19091 N-213. n-Butanol was used as internal standard.

Catalytic evaluations were carried out in duplicate with an experimental error lower than 5%. Conversion of Gly and selectivity to 1,2-PDO were calculated from chromatographic data.

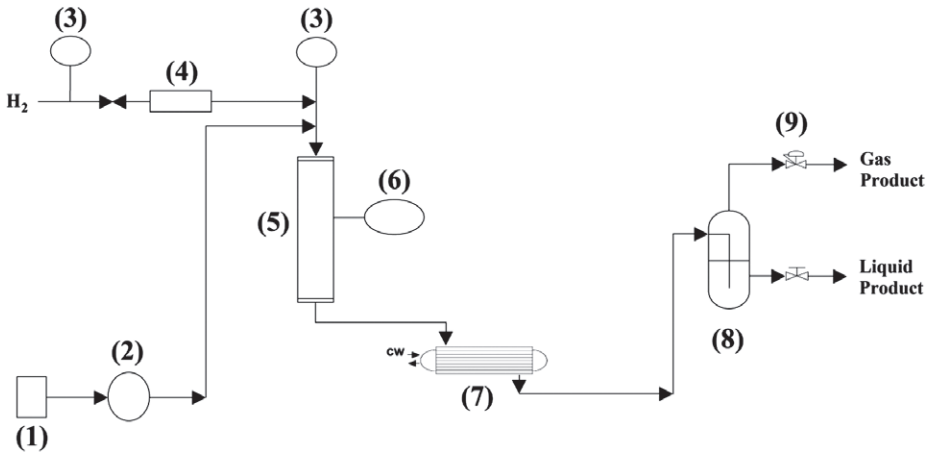

Figure 1. Diagram of the reaction equipment. (1) Liquid feed container; (2) high pressure metering pump; (3) manometer; (4) mass flow controller; (5) reactor and furnace; (6) temperature controller and display; (7) cooler/condenser; (8) high pressure gas–liquid separator; (9) backpressure regulator. CW: cooling water.

The selectivity to a particular product *i* was calculated with the following equation:

$$S_i\,(\%) = \frac{Amount\ of\ glycerol\ converted\ to\ i\ (mole)}{Amount\ of\ glycerol\ converted\ (mole)} \times 100$$

RESULTS AND DISCUSSION

Study of thermodynamically feasible reactions

A thermodynamic study is necessary to define the feasibility of the reactions that can occur in a range of operation conditions. It is also necessary to define values for equilibrium conversion and selectivity, useful for the analysis of reaction tests results. A thermodynamic study also gives information on the degree of reversibility of the reactions and the relations between them.

A literature search was performed in order to list all possible reactions occurring in the TBR.[2,30,31] A total of 20 reactions are listed in Table 1, including dehydration, hydrogenation and cracking. The change in the Gibbs free energy of reaction at 230 °C ($\Delta G°_r$) was calculated from experimental values of the energy and heat of formation at 25 °C in the gas phase ($\Delta G°_f$ and $\Delta H°_f$)[32,33] and corrected to 230 °C by means of the Gibbs-Helmholtz relation.[32] Thermodynamic properties for AOL were taken from the DIPPR database, as published elsewhere.[34] Properties of allylic alcohol and 3-hydroxypropanal ($\Delta G°_f$ and $\Delta H°_f$) were taken from another source.[35] These are estimated values calculated with Joback's method.[36] Values for acrolein were taken from the report of Lewars and Liebman[37] and values for Gly from Tapia *et al.*[38] Reactions were classified with attention to their value of Gibbs free energy, or equilibrium constant (K_{eq}), as being completely irreversible ($K_{eq} > 10$, $\Delta G°_r < -10$ kJ mol^{-1}), unfeasible ($K_{eq} < 1/10$, $\Delta G°_r > 10$ kJ mol^{-1}) and reversible ($1/10 < K_{eq} < 10$, -10 kJ mol^{-1} $< \Delta G°_r < 10$ kJ mol^{-1}).

It can be seen that most of the reactions are completely irreversible. In the case of dehydrations this is the case at any temperature of reaction and it is a consequence of the stability of water, that has a largely negative value of $\Delta G°_f$ in comparison with other degradation products of similar molecular size. Hydrogenation of AOL, 3-hydroxypropanal and propanal are reversible or unfeasible reactions at 230 °C despite being mostly irreversible at room temperature. This is due to the relatively high heat of reaction of hydrogenation and the value of the temperature of reaction. Values of K_{eq} calculated from the ΔG^0_r values for these hydrogenation reactions coincide with those reported by Huang *et al.*,[39] who performed similar calculations with Gibbs free energies in the gas phase from the ASPEN Plus Database. For AOL hydrogenation $K_{eq} = 10^{-1}$. These values moved the authors[39] to propose that an equilibrium existed between the products of the reaction of dehydration and hydrogenolysis of Gly, i.e. AOL and 1,2-PDO. Other authors, like Akiyama *et al.*[40] have indicated that hydrogenation of AOL is thermodynamically limited and that Gly conversion should be performed in two steps, one at high temperature to promote dehydration and another of lower temperature (100–120 °C) to promote hydrogenation.

Our results have indicated that total conversion of Gly and with a high selectivity to 1,2-PDO is possible. This is in contrast with the positive values of $\Delta G°_r$ of Table 1 and those reported by some authors. A more rigorous analysis indicates that the problem is the assumption of gas phase conditions for reactants and products. Since the reactions are performed in liquid media, in aqueous solution, the calculations must be corrected using the Gibbs free energy of solvation. This is defined as the difference in the free energy of a species in the gas phase and in solution. If the Gibbs free energy of the compounds is calculated in the solvated state[41] a much lower value is obtained. These contributions should drive the final value of $\Delta G°_r$ to negative values though accurate estimations cannot be provided.

With respect to the compositional analysis from chromatography data, when using a value of space velocity LHSV = 1.9 h^{-1} in the catalytic test, for any of the catalysts it was found that: (i) as found by chromatographic analysis, 1,2-PDO, AOL, PrAL, PrOH, AO, MeOH, EtOH, 3-HP and 1,3-PDO were among the reaction products; (ii) acrolein was not detected in meaningful amounts. Therefore it was assumed that reactions (10) and (18) practically did not occur at the reaction conditions used, probably because of the existence of high activation energy. Reaction (11) and (16) can also be discarded as a consequence; (iii) ethylene glycol and acetaldehyde were also not detected in meaningful amounts and for this reason, reactions (12), (13), (14) and (19) were discarded; (iv) allyl alcohol was not detected at all, hence equations (15) and (17) were discarded; (v) other reaction products, different from those of Table 1, were present only in amounts lower than 0.1% and hence were not considered for the analysis.

Table 1. Thermodynamic analysis of possible reactions. PrAL: propanal, PrOH: 1-propanol, 3-HP: 3-hydroxypropanal, AO: acetone, MeOH: methanol, EtOH: ethanol, 1,3-PDO: 1,3-propanediol, EG: ethylene glycol. Calculations performed with reactants and products in the gas phase.

Reaction type	Chemical reaction		ΔH^0_r (kJ mol^{-1})	ΔG^0_r (kJ mol^{-1})	$\Delta G^0_{r,230\,°C}$ (kJ mol^{-1})	Type
Dehydration	Gly ⇔ AOL + H_2O	**(1)**	-33.99	-72.95	-99.75	Irreversible
Hydrogenation	AOL + H_2 ⇔ 1,2-PDO	**(2)**	-59.8	-19.2	8.73	Reversible
Dehydration	1,2-PDO ⇔ PrAL + H_2O	**(3)**	-7.03	-49.73	-79.10	Irreversible
Hydrogenation	PrAL + H_2 ⇔ PrOH	**(4)**	-65.40	-34.76	-13.68	Reversible
Dehydration	Gly ⇔ 3-HP + H_2O	**(5)**	13.65	-51.97	-97.11	Irreversible
Hydrogenation	3-HP + H_2 ⇔ 1,3-PDO	**(6)**	-102.98	-33.62	14.09	Unfeasible
Dehydration	1,3-PDO ⇔ PrAL + H_2O	**(7)**	-7.03	-49.73	-79.10	Irreversible
Cracking	AO + 2 H_2 ⇔ MeOH +EtOH	**(8)**	-222.6	-178.87	-148.79	Irreversible
Dehydration	1,2-PDO ⇔ AO + H_2O	**(9)**	-32.83	-75.89	-105.51	Irreversible
Dehydration	Gly ⇔ Acrolein +2 H_2O	**(10)**	28.84	-66.98	-132.9	Irreversible
Hydrogenation	Acrolein + H_2 ⇔ PrAL	**(11)**	-125.20	-68.34	-29.22	Irreversible
Cracking	Gly ⇔ EG + H_2 + CO	**(12)**	72.97	7.25	-37.96	Irreversible
Hydrogenolysis	Gly + H_2 ⇔ EG + MeOH	**(13)**	-21.50	-17.92	-15.46	Reversible
Dehydration	EG ⇔ Acetaldehyde + H_2O	**(14)**	-18.13	-59.09	-87.27	Irreversible
Dehydration	1,3-PDO ⇔ Allyl alcohol + H_2O	**(15)**	59.97	0.81	-39.89	Irreversible
Hydrogenation	Acrolein + H_2 ⇔ Allyl alcohol	**(16)**	-58.20	-17.80	9.99	Reversible
Hydrogenation	Allyl alcohol + H_2 ⇔ PrOH	**(17)**	-132.40	-85.30	-52.90	Irreversible
Dehydration	3-HP ⇔ Acrolein + H_2O	**(18)**	15.19	-15.01	-35.79	Irreversible
Hydrogenation	Acetaldehyde + H_2 ⇔ EtOH	**(19)**	-63.30	-34.75	-15.11	Irreversible
Global	Gly + H_2 ⇔ 1,2-PDO + H_2O	**(20)**	-93.79	-92.15	-91.02	Irreversible

Notably the absence of ethylene glycol in the products of our tests was attributed to the different residence time values used in the trickle-bed experiments, in comparison with other published data, that have been obtained in batch reactors and at longer reaction times.

A simplified reaction network was thus written after disregarding the unfeasible reactions and those of negligible occurrence (see Fig. 2). The remaining nine reactions comprise dehydrations, cracking and hydrogenations.

An analysis of the values of the Gibbs free energy of reaction indicates that most of the reactions of the previous network can take place. Cracking and dehydration are completely irreversible while hydrogenations are reversible reactions limited by equilibrium.

Phase equilibrium of the reacting mixture

An assessment of the fluid phase conditions inside the reactor is very important for correctly interpreting the results of the catalytic tests. The coexistence of multiple phases can lead to the onset of interphase mass transfer resistances that decrease the global reaction rate.

One first question is that of the existence of one or two fluid phases in the reactor at the working reactor conditions. Table 2 contains data on the physical state and composition of the feedstock solution at different pressures (8–20 bar) and temperatures (210–250 °C) and at a H_2/Gly molar ratio of 10 inside the reactor. The physical (liquid or vapor) states and molar composition of each phase were inferred from vapor pressure equilibrium data for the pure compounds. This was done by using UniSim (version R430, 2013, NRTL model).

Therefore, at the studied reaction conditions three phases can be found inside the reactor, the solid phase, i.e. the catalyst, a liquid phase comprising mainly Gly and water, and a gas phase comprising mainly hydrogen and vaporized water. The concentration of water in the liquid phase depends on both the temperature and the pressure. The amount of liquid phase is decreased as the temperature of reaction is increased.

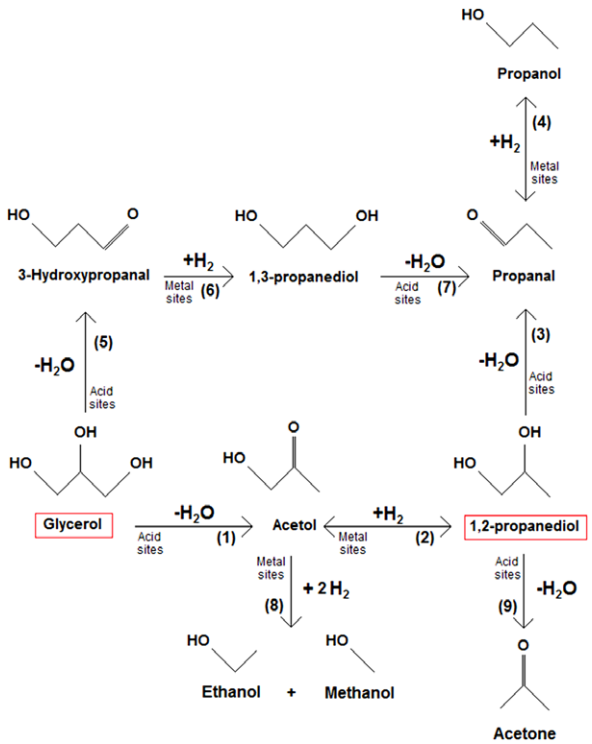

Figure 2. Simplified reaction network for the conversion of Gly.

When increasing the liquid space velocity (1.9–5.63 h^{-1}), the water molar fraction is increased in both phases, while the molar fractions of Gly and hydrogen are decreased. The amount of hydrogen in the liquid phase is almost negligible.

Table 2. Fluid phase composition, feedstock solution (80% w/w Gly in water) as a function of pressure and temperature at conditions of thermodynamic equilibrium. LHSV = 1.9 h^{-1}, H_2/Gly molar radio = 10.

			Molar flow (gmol h^{-1})		Vapor composition			Liquid composition		
T, °C	Vapor fraction	G (kg m^{-2} s^{-1})	Vapor	Liquid	Y_{H2O}	Y_{Gli}	Y_{H2}	X_{H2O}	X_{Gli}	X_{H2}
Pressure = 8 bar										
210	0.6329	0.0041	0.2234	0.1296	0.4183	0.0072	0.5745	0.2512	0.7482	0.0005
230	0.6676	0.0039	0.2357	0.1174	0.4387	0.0167	0.5446	0.1927	0.8067	0.0006
250	0.7016	0.0038	0.2477	0.1054	0.4467	0.0350	0.5182	0.1458	0.8534	0.0007
Pressure = 14 bar										
210	0.5775	0.0072	0.2039	0.1491	0.3673	0.0035	0.6293	0.3428	0.6563	0.0009
230	0.6207	0.0069	0.2191	0.1339	0.4063	0.0082	0.5854	0.2761	0.7229	0.0010
250	0.6573	0.0066	0.2320	0.1210	0.4293	0.0179	0.5529	0.2181	0.7807	0.0012
Pressure = 20 bar										
210	0.5349	0.0103	0.1888	0.1642	0.3188	0.0021	0.6790	0.4007	0.5980	0.0012
230	0.5829	0.0099	0.2058	0.1472	0.3718	0.0051	0.6230	0.3361	0.6625	0.0014
250	0.6242	0.0095	0.2204	0.1327	0.4069	0.0113	0.5818	0.2739	0.7243	0.0017

One column was eliminated because it had always the same value. G: gas superficial velocity, L (liquid superficial velocity) = 0.0402 kg m^{-2} s^{-1}.

When the H_2/Gly molar ratio is increased the vapor fraction increases. According to the simulation results for H_2/Gly molar ratios higher than 80 the system is biphasic (only solid–gas) while for values lower than 80 three phases appear (solid, liquid and gas).

Reactor fluodynamics

Inside a packed bed of particles in which there is a downward flow of a liquid and a gas, many flow patterns can be distinguished. According to Charpentier[42] the four main flow regimes observed for no foaming systems are trickle flow (T), pulsing flow (P), mist flow (M) and bubble flow (B). Each flow regime corresponds to a specific gas–liquid interaction thus having a great influence on parameters such as liquid holdup, pressure drop and mass and heat transfer rates. The trickle flow regime prevails at relatively low gas and liquid flow rates and is the preferred mode in industrial practice.

Knowledge of the prevailing flow regime, pressure drop, and liquid holdup are considered essential for the design and performance evaluation of a trickle-bed reactor (TBR). For this reason there have been multiple efforts to model their hydrodynamics. The existing flow pattern is found to depend on the superficial velocities of the gas (G) and the liquid (L). According to Tosun[43] the regime of a TBR is that of 'trickling' flow when L is lower than 10 and G is lower than 10^{-1} (both in kg m^{-2} s^{-1}).

Inspection of the G and L values of Table 2 indicates that for all conditions in this work the reactor flow pattern is "trickling".

Physicochemical properties of the catalysts

Table 3 shows the results of the characterization of the catalysts and the support. ICP chemical analysis confirmed the theoretical amount of metal Cu in the prepared catalyst (CA) within a 5% error. The composition of the copper chromite (CC) catalyst is more complex since, besides Cu, other elements are present: Cr, Na, P and Mn.

After being calcined at 500 °C, the Al_2O_3 support had a specific surface area of 180 m^2 g^{-1} and a pore volume of 0.387 cm^3 g^{-1}. Cu addition (CA catalyst) modified the textural properties of the Al_2O_3 support. CA had a specific surface area of 141.8 m^2 g^{-1} and a pore volume of 0.361 cm^3 g^{-1}. Figure 3 shows the pore size distribution

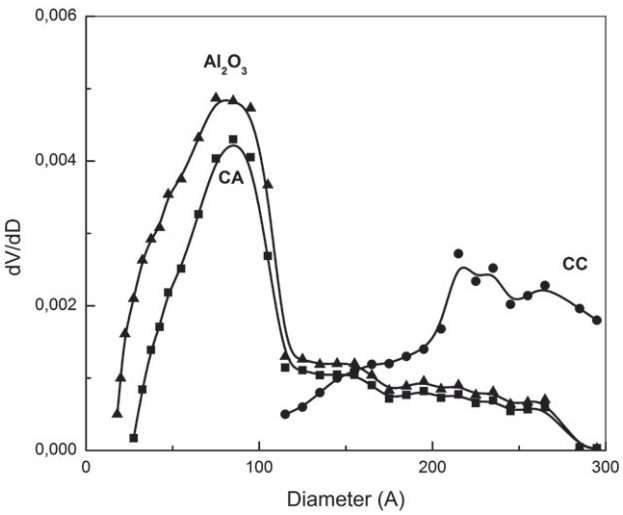

Figure 3. Pore size distribution of the support and the CA and CC catalysts.

of the support and the catalysts. The support had a unimodal pore size distribution spanning the 20–120 Å range and centered at 75 Å. CA had a unimodal pore size distribution in the 20–120 Å range and centered at 85 Å. Considering a solid density (alumina) of 3.95 g cm^{-3}, the pellet density is calculated as 1.63 g cm^{-3} and the pellet porosity as 0.59.

It can be seen that the CC catalyst had the lowest surface area of the two catalysts. The CC catalyst had a specific surface area of 20.8 m^2 g^{-1}, a pore volume of 0.25 cm^3 g^{-1} and a pore size distribution centered around 225 Å. Considering a solid density ($Cu_2Cr_2O_5$) of 4.5 g cm^{-3}, the pellet density is calculated as 2.1 g cm^{-3} and the pellet porosity as 0.53.

The X-ray diffraction (XRD) pattern of the Al_2O_3 support had the typical signals of the gamma phase of alumina: 37.7°, 45.9° and 66.9°.[44] The X-ray diffractograms of the catalysts are shown in Fig. 4. Peaks corresponding to CA can be seen at $2\theta = 35.6$, 38.6, 47, 53.5, 58.2, 62, 66.2, 68 and 75°. This is consistent with JCPDS data assigned to CuO (JCPDS 41-254) and with reports of Durán-Martín *et al.*[45] The peak located at $2\theta = 45.9°$ corresponds with the alumina support.

Table 3. Physicochemical properties of catalysts.

Catalyst	Composition, %					Sg_{BET} ($m^2\ g^{-1}$)	V_{poro} ($cm^3\ g^{-1}$)*
	Cu	Cr	Mn	Na	P		
Al_2O_3	-	-	-	-	-	180	0.387
CC	29.5	22.8	0.0079	3	1.6	20.8	0.330
CA	12.8	-	-	-	-	141.8	0.250

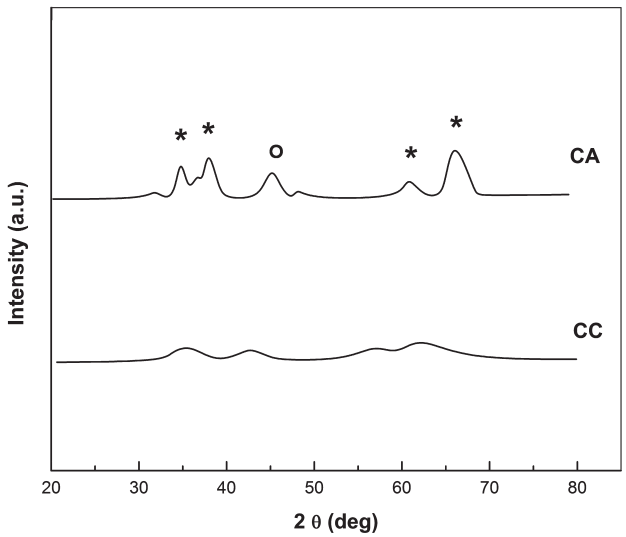

Figure 4. X-ray diffractograms of the CA and CC catalysts without treatment. Identified phases: CuO (☆)[43,44] and γ-Al_2O_3 (○).[42]

The XRD results show that CC is an amorphous catalyst where the intensity of the crystalline phases is very low. This suggests that the CuO phase is quasi-amorphous and/or formed by small crystalline domains that are not detectable by XRD.[46]

Besides, this copper oxide phase is formed by large crystallites with a medium size of about 77.8 Å for CA, as calculated by the Debye–Scherrer equation.

The temperature programmed reduction (TPR) traces of the catalysts are included in Fig. 5. Two reduction peaks can be distinguished in both cases. The catalyst with low copper loading (CC) has one peak centered at about 232 °C and a second smaller one at about 279 °C. CA also has two peaks, of the same intensity. Larsson *et al.*[47] reported the presence of two reduction peaks for the Cu/γ-Al_2O_3 catalysts (4 wt.% and 12 wt.% Cu), one at 230 °C and a second one at 270 °C, and assigned the first peak to the reduction of well-dispersed copper alumina surface species and the high temperature peak to the reduction of bulk CuO. In summary, the results show that the reduction of CuO on the samples started at a temperature around 200 °C and was completed at about 310 °C. Some authors have reported that peaks at around 225–230 °C can be attributed to the reduction of Cu^{2+} species, well-dispersed CuO particles, to metallic copper (Cu^0). Then the shoulder could be related to the reduction of Cu^{2+} in large CuO particles.[42,46]

The XRD and TPR results indicate the presence of oxidized Cu species (CuO) on the surface of the catalysts. After the reduction treatment at 250 °C, before the reaction test, reduced Cu species would be obtained (Cu^0 y Cu^+) that could act as active sites for hydrogenolysis.[7]

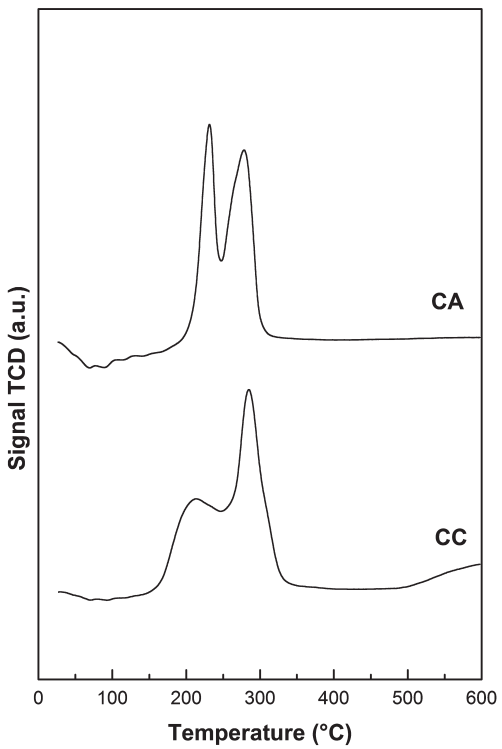

Figure 5. TPR traces of the studied catalysts.

X-ray photoelectron and Auger electron spectra of the CA and CC catalysts treated in H_2 (250 °C, 1 h) can be seen in Fig. 6. In both samples, the binding energy of the Cu $2p_{3/2}$ peak appears at 932.3 eV (Fig. 6(a)), which could correspond to both Cu^0 and Cu^+ species. The presence of Cu^{2+} is discarded, as evidenced by the absence of a satellite peak at *c.* 942.9 eV.[48,49] The Auger Cu_{LMM} spectra (Fig. 6(b)) permits elucidation of the identity of the copper species. A broad peak centered at 919.0 eV for both samples suggests the presence of Cu^0.[45] The CC catalyst exhibits an additional small peak at about 916.8 eV, indicating the presence of a minor concentration of Cu^+ species. In summary XPS and Auger spectra of the samples demonstrate the dominant presence of metallic copper (Cu^0) on the catalyst surface. A much lower amount of Cu^+ is also detected in the CC catalyst.

The XPS results indicate that the Cu species were totally reduced after the hydrogen treatment. Cu^0 crystals were likely the most abundant species on the surface of the catalysts.

Thermal programmed desorption (TPD) of pyridine is a technique that gives information about the total acidity of catalysts, and of the distribution of acid strength. The area under the pyridine TPD trace is proportional to the total acidity.[29] Acid sites on a catalyst can be classified as weak, medium or strong depending on the temperature range in which pyridine is desorbed. Weak

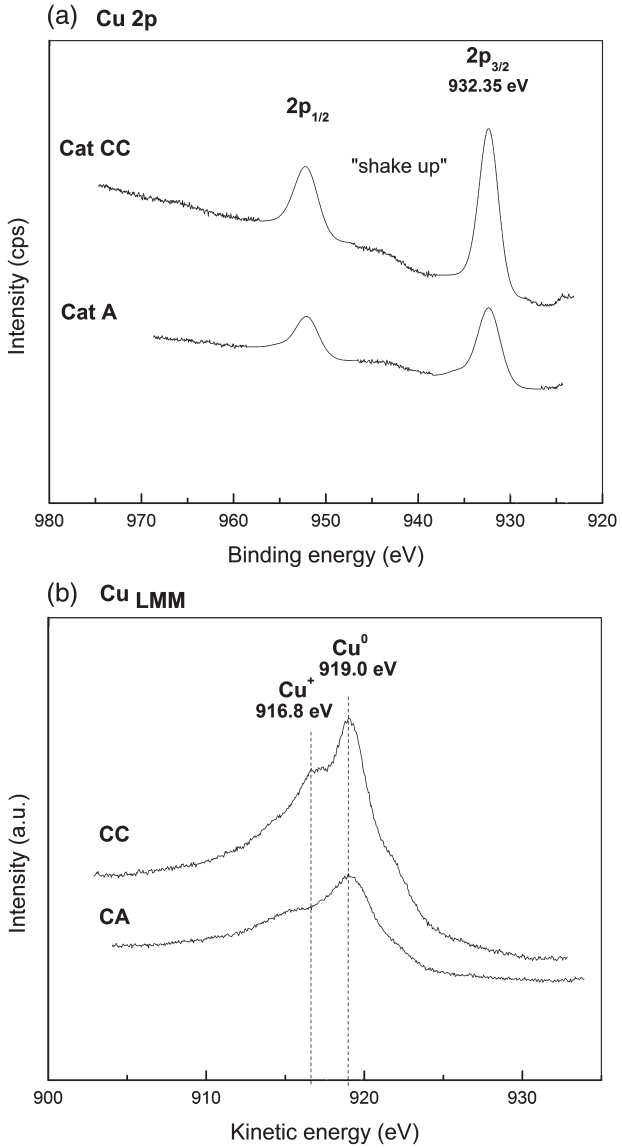

Figure 6. Cu 2p XPS (a) and Cu_{LMM} Auger (b) spectra. CA and CC catalysts treated in H_2 at 250 °C for 1 h.

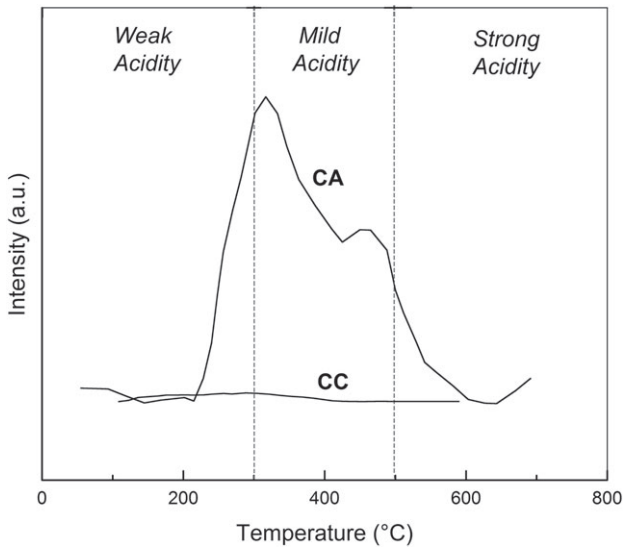

Figure 7. Results of pyridine thermal programmed desorption (TPD).

acid sites desorb in the temperature range 150–300 °C. Mild acid sites desorb pyridine between 300 and 500 °C and strong acid sites between 500 and 650 °C.[50] Figure 7 shows the results obtained for both catalysts. It can be seen that CC has practically no acid sites while CA has an important level of acidity. For CA two peaks can be clearly distinguished at 320 and 460 °C. These two peaks correspond to sites of mild acidity. The results indicate that CA has mainly sites of mild acidity (about 70%) and a small concentration of weak acid sites (20%) and strong acid sites (10%). These results correlate with data reported elsewhere.[51,52]

TEM micrographs of the copper chromite (CC) and alumina supported copper (CA) catalysts are included in Fig. 8. Identification of the particles was easy for the CA catalyst but impossible for the CC catalyst. This is understandable since CA is a supported catalyst with high support-metal contrast while CC is a bulk catalyst with absorption from both Cu and Cr. The arithmetic mean particle diameter for CA was 4.6 nm. The volume/area mean diameter was 4.7 nm. Considering all experimental errors the diameter value had an associated error of ±7%. Counting of the particles and measurement of their diameters permitted a narrow histogram to be obtained: 3–4 nm (25%), 4–5 nm (58%) and 5–6 nm (29%).

For the CA catalyst, if a semispherical particle shape is assumed, a metal dispersion of about 23% can be calculated. In global terms there are 0.48 mmol surface Cu atoms per gram of catalyst. In the case of the copper chromite catalyst, although TEM micrographs yielded no information, the number of exposed surface atoms can be estimated from the Cu surface density of copper chromite (about 6.2 Cu nm^{-2}) and the measured specific surface area (20.8 $m^2\ g^{-1}$). This amounts to 0.21 mmol surface Cu atoms per gram of catalyst.

The characterization results indicate that the two catalysts are very different. CA has a copper content much lower than that of CC (12.8% compared with 29.5%). CC contains also other metals (Cr, Mn, Na and P). The specific surface area of CA is almost an order of magnitude higher than that of CC (141.8 and 20.8 $m^2\ g^{-1}$). Both have a unimodal pore size distribution, centered at 85 Å in the case of CA and at 225 Å in the case of CC. With regard to the crystalline structure, CA contains copper crystals in the monoclinic habitat while CC is quasi-amorphous. Finally the acidity of CC is practically null while CA has medium acidity, with sites of mainly medium acid strength.

Most literature reports indicate that alcohol dehydration demands sites of medium acid strength. If a mechanism of two reactions in series is considered, with dehydration as the first one, very little catalytic activity should be expected in the case of CC catalyst, because its acid activity is negligible[53]. This issue will be considered in the following sections.

Glycerol hydrogenolysis results

Gaseous products were analyzed in a gas chromatograph using the same conditions for the analysis of the liquid phase. The gas phase was composed almost exclusively of hydrogen and quantification of the organic compounds indicated that they had a negligible contribution to the carbon balance. An overall mass balance was made by weighing the feed as well as the reactor effluent. The carbon balance was closed up to 100 ± 4% for two runs performed with the CA and CC catalysts.

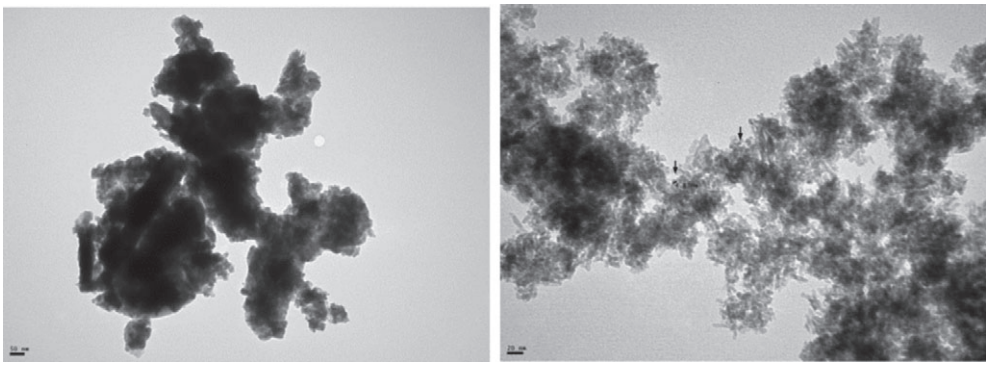

Figure 8. TEM micrograph of the CC catalyst (left) and the CA catalyst (right).

Figure 9 shows results of Gly hydrogenolysis as a function of time-on-stream. Values of Gly conversion and selectivity to 1,2-PDO are plotted for both catalysts at 230 °C, 14 bar, LHSV = 1.9 h^{-1}, molar ratio H_2/Gly = 10. Total conversion of Gly and high selectivity values to 1,2-PDO (>95%) were obtained for both catalysts. During the experiments the catalysts did not suffer deactivation. The results obtained let us infer that:

1 Both catalysts show high activity and selectivity to the desired product of reaction, 1,2-PDO. Only minor amounts of other byproducts are detected. Referring to Fig. 2 almost exclusively reactions 1 (dehydration of Gly to AOL) and 2 (hydrogenation of AOL to 1,2-PDO) take place.
2 As can be seen in Fig. 8 and in spite of their very different physical properties, both catalysts display similar values of selectivity to 1,2-PDO. At values of time-on-stream higher than 2 h, high values of selectivity to 1,2-PDO and conversion of Gly (> 95%) can be seen. In the case of the CC catalyst the values of selectivity to 1,2-PDO and total conversion of Gly are 65% and 79% in the first hour of time-on-stream and grow continuously to stable values at 4 h (total conversion and about 95% selectivity). These results could be explained by assuming that both catalysts have the same kind of active sites, i.e. that the catalytic activity is related to the presence of Cu^0 species.

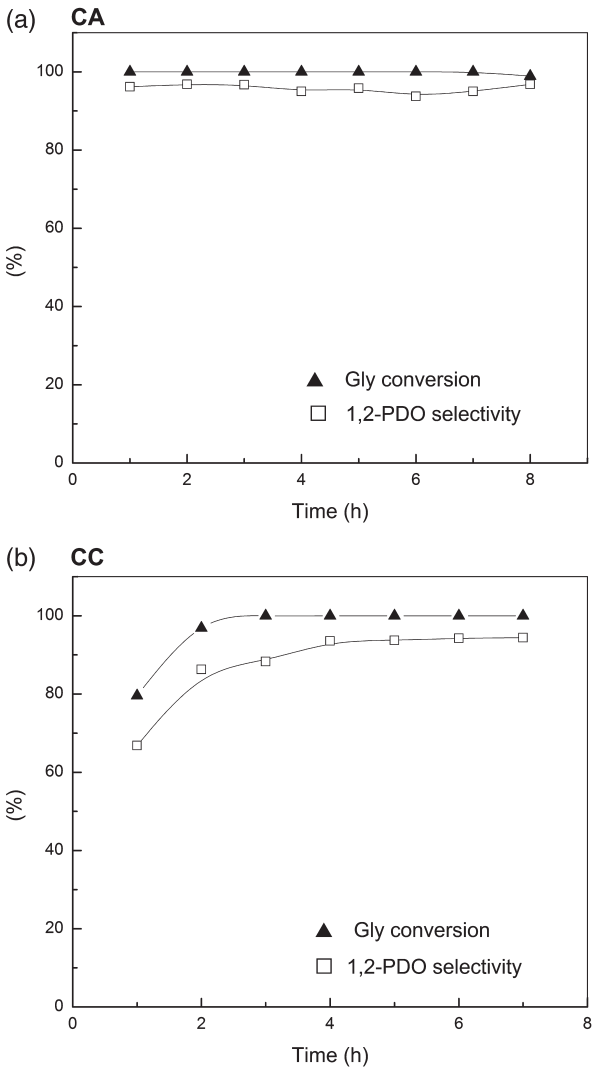

Figure 9. Conversion and selectivity to 1,2-PDO as a function of time-on-stream for the two studied catalysts: (a) CA; (b) CC.

Mass and heat transfer phenomena

Mass and heat transfer phenomena can greatly modify the catalytic properties. Checking the existence of these kinds of limitations is of great importance because they can affect the global chemical reaction rate and selectivity. For hydrogen or Gly to reach the catalyst surface a series of mass transfer stages must be passed. This leads to the formation of different concentration gradients in the different phases. The resistance to heat and mass transfer of each of these stages can be estimated theoretically from fundamental relations and from measured data.

The average experimental reaction rate was calculated from the value of conversion of Gly and the Gly feed molar flowrate. The average reaction rate per unit mass of catalyst, $\hat{r}_{Gly}$, was used.

$$\hat{r}_{Gly} = \frac{X_{Gly}}{W/F^0_{Gly}} \quad (1)$$

$\hat{r}_{Gly}$ is obviously smaller than the local reaction rate at the entrance of the reactor, where $X \sim 0$, and should be higher than the local reaction rate at the exit, where X is maximum. In order to gain insight to the magnitude of the different resistances (gas–liquid, liquid–solid, diffusion–reaction), reaction tests at different values of F^0_{Gly} (0.115–0.342 mL min^{-1}) were made, while keeping the reaction temperature *(T)*, catalyst mass and particle size *(R_p)* constant (210 °C, 4 g and 0.18 mm, respectively).

The results in Fig. 10 indicate that the average reaction rate was insensitive to the residence time (residence time proportional

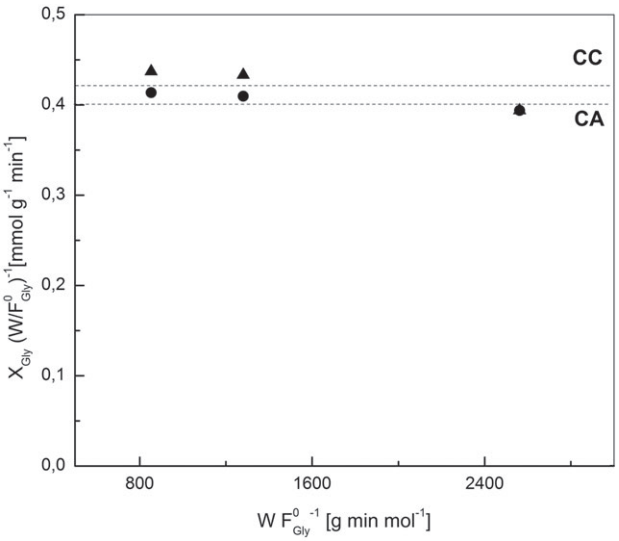

Figure 10. Average reaction rate per unit catalyst mass as a function of the ratio (W/F^0_{Gly}): (a) CA; (b) CC.

to W/F^0_{Gly}). Moreover the reaction rate seemed to be constant. If we take into account that the points of Fig. 9 correspond to experiments with final Gly conversion values between 20 and 90%, the system behaves like a reactor with a reaction of zero order (with respect to Gly). These results could point to a rate controlling mechanism that depends on hydrogen, hydrogen pressure being approximately constant. These aspects will be inspected in the following paragraphs, in which chemical reaction, solid–liquid and gas–liquid resistances will be calculated. Properties of the catalysts for these calculations are included in Table 4 and fluid properties in Table 5.

Dilution of the bed was accomplished by mixing the catalyst particles with other SiC particles of similar or slightly bigger size. Both dilution and use of a small particle size had the objective of improving the wetting of the catalysts that was considered to be complete.

Effective diffusivities were estimated with the Wilke-Chang equation[54] for molecular diffusion of molecules in liquids and correcting by the porosity factor. Since diffusion occurs inside the pores filled with liquid, Knudsen diffusion was deemed irrelevant. Tortuosity and constriction factors were also disregarded. In this sense, the effective diffusivity calculated is an upper estimate.

$$D_e = \varepsilon\, D_M \tag{2}$$

At any point in the reactor and at steady state conditions, the flow of Gly or hydrogen between the different phases should be the same. In this sense, Equation (3) should apply:

$$r_{H2} = r_{Gly} = -\frac{dN_{H2}}{dV} = -\frac{dN_{Gly}}{dV} = f\left(C_{S,H2}, C_{S,Gly}, T_S\right) \tag{3}$$

$$\bar{r}_{H2} = Q_{L\to S,H2} = Q_{G\to L,H2} \tag{4}$$

$$\bar{r}_{Gly} = Q_{L\to S,Gly} \tag{5}$$

The value of r_{H2} and r_{Gly} for estimation of the mass transfer resistances will be calculated from the value of $\hat{r}_{Gly}$, the average rate of consumption of Gly per unit mass of catalyst.

$$r_{Gly} = \hat{r}_{Gly}\,\rho_p \qquad \left(\text{per unit volume of catalyst}\right) \tag{6}$$

$$\bar{r}_{Gly} = r_{Gly}\,\left(1-\varepsilon_B\right)\chi \qquad \left(\text{per unit volume of reactor}\right) \tag{7}$$

From Fig. 10 a value 0.41 mmol min^{-1} g^{-1} reaction rate per unit catalyst mass can be read. This translates to r_{Gly} equal to 0.67 mmol min^{-1} cm^{-3} for the CA catalyst and 0.86 for the CC catalyst. For the rate per unit volume reactor, use of Equation (7) yields values of 0.2 mmol min^{-1} cm^{-3} for CA and 0.26 mmol min^{-1} cm^{-3} for CC. The molar fluxes Q_G and Q_L are descripted from known correlations for the film transfer coefficients k_c and K_L.

$$Q_{G\to L,H2} = K_{L,H2}a_g\left(\frac{C_{g,H2}}{H} - C_{L,H2}\right) \tag{8}$$

$$Q_{L\to S,H2} = k_{c,H2}a_c\left(C_{L,H2} - C_{S,H2}\right) \tag{9}$$

$$Q_{L\to S,Gly} = k_{c,Gly}a_c\left(C_{L,Gly} - C_{S,Gly}\right) \tag{10}$$

$C_{L,H2}$ and $C_{L,Gly}$ are the bulk concentrations of dissolved hydrogen and Gly in the liquid phase. $C_{g,H2}$ is the bulk concentration of hydrogen in the gas phase. H is Henry's constant for dissolution

Table 4. Geometrical and physical data of the catalysts and catalyst bed.

Property	Value	Units	Description	Comments
ρ_A	3.95	g cm^{-3}	Alumina density	Non-porous solid
ρ_{CA}	1.63	g cm^{-3}	Cu/Al_2O_3 catalyst pellet (CA) density	Measured
ρ_{CC}	2.1	g cm^{-3}	Chromite copper catalyst pellet (CC) density	Measured
$V_{g,CA}$	0.36	cm^3 g^{-1}	Cu/Al_2O_3 catalyst pellet pore volume	Measured
$V_{g,CC}$	0.33	cm^3 g^{-1}	Chromite copper catalyst pellet pore volume	Measured
ε_B	0.4	dimensionless	Bed porosity	Measured
d_p	0.36	mm	Particle diameter	Measured
ε_{CA}	0.59	dimensionless	Porosity of the CA catalyst pellet	Calculated
ε_{CC}	0.53	dimensionless	Porosity of the CC catalyst pellet	Calculated
a_c	167	cm^2 cm^{-3}	Area per unit volume of catalyst pellet	Calculated
k_e	0.005	kCal s^{-1} cm^{-1} K^{-1}	Effective thermal conductivity, catalyst pellet	Alumina, reported
χ	0.5	m^3 m^{-3}	Volumetric dilution factor (inert solid particles)	Calculated
$\rho_{B,CA}$	0.49	g cm^{-3}	Catalyst bed density, copper over alumina	Measured
$\rho_{B,CC}$	0.63	g cm^{-3}	Catalyst bed density, copper chromite	Measured

Table 5. Relevant fluid properties for calculation of the mass transfer resistances. The liquid phase is an 80:20 Gly:water solution. Liquid diffusivities were estimated with Wilke's law. Gas diffusivities were interpolated from experimental data with Hirchsfelder's law, i.e. $D \alpha P^{-1} T^{3/2}$ [54].

Property	Value	Units	Description	Observations
ρ_L	1.21 / 1.08	g cm^{-3}	Density of glycerol:water (80:20) solution [55]	25 °C/230 °C
u_L	0.0059	cm s^{-1}	Fluid phase velocity, inside the reactor	230 °C
$C_{L,Gly}$	10.4	mol L^{-1}	Concentration of glycerol, liquid phase	Reactor feed
C^{eq}_{L,H_2}	0.23	mmol L^{-1}	H_2 concentration in 80:20 glycerol:water [56]	25 °C, 1 atm
H	0.06-0.09	GPa (mol fraction)$^{-1}$	Henry's constant for hydrogen dissolved in methanol, ethanol and propanol [57]	230 °C
H	0.20	GPa (mol fraction)$^{-1}$	Henry's constant for hydrogen dissolved in tetraethyleneglycol [58]	230 °C
C^{eq}_{L,H_2}	157	mmol L^{-1}	Equilibrium hydrogen concentration, liquid phase, for adopted $H = 0.1$ GPa (mol fraction)$^{-1}$	Estimated, 230 °C, 14 atm
μ_L	1.931	cP	Viscosity liquid phase, UniSim Design	Estimated, 230 °C
μ_L	3.18	cP	Glycerol:water (80:20) solution viscosity [55]	Reported, 100 °C
F^L_v	1.22×10^{-5}	m^3 h^{-1}	Liquid volumetric flow rate	230 °C, 14 atm
ΔH_H	−89	kJ mol^{-1}	Heat of reaction of hydrogenolysis of glycerol to propanediol	From Table 1
$D^{H2}_{M,G}$	0.668–1.747	cm^2 s^{-1}	Gas diffusivity, hydrogen in air [59]	Reported, 0–200 °C, 1 atm
$D^{H2}_{M,G}$	1.25×10^{-1}	cm^2 s^{-1}	Gas diffusivity, hydrogen	Estimated, 230 °C, 14 atm
$D^{H2}_{M,L}$	4.50×10^{-5}	cm^2 s^{-1}	Hydrogen (dis) molecular diff. in liquid water [60]	25 °C
$D^{H2}_{M,L}$	4.08×10^{-5}	cm^2 s^{-1}	Hydrogen (dis) mol. Diff. liquid phase, Wilke eq. [54]	Estimated, 230 °C
$D^{Gly}_{M,L}$	1.76×10^{-5}	cm^2 s^{-1}	Glycerol mol. Diffusivity, liquid phase, Wilke eq. [54]	Estimated, 230 °C
$D^{H2}_{e,L}$	$2.41 - 2.16 \times 10^{-5}$	cm^{0032} s^{-1}	Intrapellet effective hydrogen diffusivity, CA-CC	Calculated, 230 °C
$D^{Gly}_{e,L}$	$1.04 - 0.93 \times 10^{-5}$	cm^2 s^{-1}	Intrapellet effective hydrogen diffusivity, CA-CC	Calculated, 230 °C

of hydrogen in the liquid phase. Some care must be taken when calculating the fluxes because a_g and a_c, the interfacial areas per unit volume, are calculated from correlations and they might have different volume basis (per unit volume catalyst, per unit volume reactor, etc.). In this sense, Equations (6) and (7) should be remembered.

Goto *et al.*[61] proposed a correlation for k_c (see equation below). a_c is the external surface area of the catalyst particle per unit reactor volume. The units of k_c are cm min^{-1} and those of a_c, cm^2 cm^{-3}.

$$k_c a_c = j_D \left[\frac{6 u_L \left(1-\varepsilon_B\right) \chi}{d_p}\right] \left(\frac{\mu_L}{\rho_L D}\right)^{-2/3} \tag{11}$$

$$j_D = 1.31\, Re_{L,p}^{-0.436} \tag{12}$$

$$Re_{L,p} = \frac{u_L\, \rho_L\, d_p}{\mu_L} \tag{13}$$

$$R_{L-S} = \frac{1}{k_c a_c} \tag{14}$$

Calculations with values from Tables 4 and 5 yield values of $R_{L\text{-}S,H2} = 0.384$ min and $R_{L\text{-}S,Gly} = 0.673$ min. In the case of the gas–liquid mass transfer (Equation (8)) the overall gas–liquid mass transfer coefficient K_L can be expressed as a combination of the coefficients on the gas side (k_g) and liquid side (k_L).

$$\frac{1}{K_L} = \frac{1}{H\, k_G} + \frac{1}{k_L} \tag{15}$$

$$H = C_G^{eq} / C_L^{eq} \tag{16}$$

H is Henry's equilibrium constant for gas dissolution in the liquid, in this case, for hydrogen in aqueous Gly, and C_G and C_L are concentrations in the gas and liquid phase. For scarcely soluble gases such as hydrogen, the values of Henry's constant are much greater than unity. It can also be considered that the term $H\, k_g$ is at least one order of magnitude greater than k_L for most values of the gas and liquid velocities found in trickle-bed reactors.[62] Taking these assumptions into account we can disregard the gas side resistance.

$$K_L a_g \cong k_L a_g \tag{17}$$

$$R_{G-L} = \frac{1}{k_L a_g} \tag{18}$$

a_g is the gas–liquid interfacial area per unit reactor volume. $R_{G\text{-}L}$ is the gas–liquid mass transfer resistance. For estimation purposes the equations of Turek and Lange can be used[63] (see equations below). D_L is the diffusivity of the dissolved gas in the liquid phase. Equation (19) for mass transfer in packed bed at low Reynolds number and without reaction yields a value for $R_{G\text{-}L}$ of 4.6 min.

$$k_L\, a_g = 16.8\, Ga^{-0.22}\, Re_{L,t}^{0.25}\, Sc_L^{0.5} \tag{19}$$

$$Ga = \frac{d_p^3\, g\, \rho^2}{\mu^2} \tag{20}$$

$$Sc_L = \frac{\mu_L}{\rho_L\, D_L} \tag{21}$$

$$Re_{L,t} = \frac{u_L\, \rho_L\, d_t}{\mu_L} \tag{22}$$

According to Equation (8), the maximum mass transfer rate, for severe mass transfer limitations and negligible dissolved gas concentration, $Q_{G\text{-}L,max}$, is equal to $C^{eq}_{L,H_2} / R_{G\text{-}L}$. This is equal to

Table 6. Summary of estimated resistances in the reacting system of the hydrogenolysis of Gly in a three phase trickle bed reactor.

Resistance	H_2	Gly
Intrapellet diffusion and reaction (R_{D-R}), min	-----	0.083
Liquid–solid mass transfer (R_{S-L}), min	0.38	0.67
Gas–liquid mass transfer (R_{G-L}), min	0.83–4.6	-----

0.034 mmol cm^{-3} min^{-1}. If we recall that $\bar{r}_{Gly}$ was 0.2–0.26 mmol cm^{-3} min^{-1}, it becomes obvious that the rate of transformation of *Gly* reaches the limit of possible mass transfer of hydrogen from the gas to the liquid phase. The value mismatch between $Q_{G-L,max}$ and $\bar{r}_{Gly}$ must be caused by underestimation of the mass transfer coefficient by Equation (19) as indicated by Turek and Lange[63] for the cases of mass transfer with simultaneous reaction, due to the effect of microturbulence and reduction of the effective size of the boundary layers, not present in the experiments without reaction. The same authors provide plots of corrected values of the mass transfer coefficient obtained in the reaction of hydrogenation of methylstyrene to cumene but they have great dispersion. Taking the $k_L a_g$ values from the report of Metaxas and Papayannakos[64] for hydrogenation in trickle bed reactors, a value for R_{G-L} of 0.83–1.66 min can be obtained.

Finally, an estimation of the intrapellet diffusion–reaction resistance should be made. The combination of reaction resistance and the intrapellet diffusion makes up the total diffusion–reaction resistance that can be compared with the other resistances of the system, R_{G-L} and R_{S-L}.

$$R_{D-R} = \frac{1}{\xi\, k} \tag{23}$$

$$\xi = \frac{\tanh(h)}{h} \tag{24}$$

$$h = \frac{d_p}{6}\sqrt{\frac{k_v}{D_e}} \tag{25}$$

h is the Thiele modulus and can be calculated from information of the kinetic constant k_v and the intrapellet effective diffusivity. In the way it is written k_v is the pseudo-first-order kinetic constant of the reaction. If we consider that the rate of hydrogenolysis of *Gly* to 1,2-PDO is first-order with respect to the concentration of *Gly*:

$$r_{H2} = r_{Gly} = -\frac{dN_{H2}}{dV} = -\frac{dN_{Gly}}{dV} = k_{v,Gly}\, C_{S,Gly} \tag{26}$$

Zhou *et al.*[17] studied the hydrogenolysis of *Gly* over copper catalysts. Their model used a first-order dependency on Gly concentration for the slow reaction of Gly to AOL. They found that the system was insensitive to hydrogen pressure, though they postulated that hydrogenation was first-order in AOL and hydrogen. A value of $k_{v,Gly} = 15.6\ min^{-1}$ at 483 K can be calculated from their reported kinetic parameters if adsorption terms are disregarded as a first approximation. The calculated Thiele modulus is then about 0.95, efficiency 0.8 and R_{D-R} about 0.083 min. A comparison of all resistances can now be written in Table 6.

Inspection of the values of Table 6 indicates that $R_{G-L} > R_{S-L} > R_{D-R}$. Since the gas–liquid and liquid–solid resistances dominate and these resistances are not a function of Gly concentration, and since the pressure of hydrogen is practically constant throughout the reactor, the overall rate of reaction is dictated by the mass transfer of hydrogen only. This fact explains the relatively constant values of the apparent global reaction rates (Fig. 9). This also explains the small influence of the kind of catalyst on the measured catalytic activity.

One underlying assumption in the calculation of R_{D-R} is that the catalyst particle is isothermal. This should also be verified, given the relatively high heat of reaction of all hydrogenation reactions. One criterium is that of assessing the maximum possible temperature difference between the surface and the center of the particle, as elucidated by Prater.[65]

$$\Delta T_{max} = T - T_S = \frac{-\Delta H_H D_e C_S}{k_e} \tag{27}$$

where ΔH_H is the heat of the hydrogenolysis reaction and C_S is the concentration at the surface. k_e is the effective thermal conductivity. An upper estimate of ΔT_{max} is calculated when using $C_S = C_{Gly,S} = C_{Gly,L} = 0.0104\ mol\ mL^{-1}$. Then Equation (27) yields ΔT_{max} lower than 1 K. Similar results of negligible ΔT are obtained if concentration and diffusivities are those of hydrogen. The particles are then isothermal.

Study of reaction conditions

Influence of the reaction temperature

The effect of reaction temperature was studied in the range 210–250 °C and the results are shown in Table 7. From analysis of the table the following conclusions can be drawn:

1. The reaction temperature does not have a significant effect on *Gly* conversion since for all temperatures used (with the exception of catalyst CC at 210 °C, $X_{Gly} = 85\%$), both catalysts convert *Gly* completely. This might indicate that the catalyst mass was in excess.
2. The selectivity to 1,2-PDO reaches values higher than 96% at the two lower temperatures studied (210 and 230 °C) on both catalysts. The second product is AOL.
3. In the tests at T = 250 °C the main reaction products are 1,2-PDO and AOL. The rest of the products formed differ in concentration depending on the catalyst used. Over CC mainly 3-HP and 1,3-PDO (reactions (5) and (6)) are formed. Over CA mainly AOL hydrogenation products appear (EtOH and MeOH) (reaction (8)) and products of dehydration of 1,2-PDO (AO) (reaction (9)).

The pattern of reaction products obtained seems to obey the network proposed in the beginning (Fig. 2). As indicated, modifying the reaction temperature should affect the products distribution. A temperature increase benefits mainly the dehydration reactions, which have an exponential dependence, in comparison with hydrogenation rates, which are limited by liquid–gas mass transfer and have a linear dependence. On the commercial catalyst 3-HP and 1,3-PDO are favored by a temperature increase while over the CA catalyst the reactions to AOL and 1,2-PDO are favored. This difference could be related to the different acidity of the catalysts.

If a scheme of consecutive reactions, all of them of first order, is proposed ($A \rightarrow B \rightarrow C$, A = Gly, B = AOL, C = 1,2-PDO), the selectivity to 1,2-PDO can be written as follows:

$$S_{1,2-PDO} = \frac{k_2}{k_1} \cdot \frac{C_{L,H_2}}{C_{L,Gly}} \cdot \frac{\xi_2}{\xi_1} \tag{28}$$

Table 7. Conversion of Gly and selectivity to reaction products at different temperatures. Time-on-stream = 8 h. Pressure = 14 bar, LHSV = 1.9 h^{-1}, molar ratio H_2/Gly = 10.

	Selectivity, %									
T, °C	AO	MeOH	EtOH	PrOH	AOL	3-HP	1,3-PDO	1,2-PDO	PrAL	Gly conversion, %
Catalyst CC										
210	nd	nd	nd	nd	3.1	nd	nd	96.9	nd	85
230	nd	nd	nd	nd	3.7	nd	nd	96.3	nd	100
250	3.3	nd	2.3	1.7	27.5	14.1	16.1	31.4	3.6	100
Catalyst CA										
210	nd	nd	nd	nd	3.2	nd	nd	96.8	nd	100
230	nd	nd	nd	0.2	2.1	0.3	0.6	96.8	nd	100
250	17	11.1	8.4	nd	25.1	nd	1.2	36.2	1	100

Table 8. Conversion of Gly and products selectivity at different pressure values. Time-on-stream = 8 h.

	Selectivities, %									
P, Bar	AO	MeOH	EtOH	PrOH	AOL	3-HP	1,3-PDO	1,2-PDO	PrAL	Gly conversion, %
CC catalyst										
8	1.4	nd	nd	nd	29.1	1.6	4.2	63.7	nd	98.2
14	nd	nd	nd	nd	3.7	nd	nd	96.3	nd	100
20	nd	nd	nd	nd	0.2	nd	4.4	95.4	nd	100
CA catalyst										
8	nd	nd	nd	nd	6.5	7.1	6.3	80.1	nd	100
14	nd	nd	nd	0.8	0.9	0.9	0.6	96.8	nd	100
20	nd	nd	nd	0.8	0.1	nd	4.0	95.1	nd	100

According to previous reports, it can be considered that $k_2 \approx k_L a_g$, because the system is governed by the gas–liquid mass-transfer. So that Equation (28) can be written as follows:

$$S_{1,2-PDO} = \frac{k_L a_g}{k_1} \cdot \frac{P}{C_{L,Gly} RTH} \cdot \frac{\xi_2}{\xi_1} \tag{29}$$

Then according to the previous equation when the temperature is increased the ratio $k_L a_g / k_1$ is decreased and the selectivity to AOL is favored. The concentration of hydrogen in the liquid phase C_{L,H_2} increases due to decrease of the gas–liquid resistance, though this has a low effect on selectivity. These trends can be clearly seen in the results previously considered (Table 7) and also coincide with others reported in the scientific literature.[66,67]

Effect of system pressure

The effect of hydrogen pressure was studied in the range 8–20 bar. Pressure was varied while the other reaction variables were kept constant (T = 230 °C, LHSV = 1.9 h^{-1}, H_2/Gly = 10). From the analysis of Table 8 the following conclusions were drawn:

1. As was the case with the reaction temperature, the system pressure has no significant effect on the conversion of Gly. For all studied pressure values Gly conversion was complete (with the exception of the catalyst CC at 210 °C, X_{Gly} = 98.2%).
2. The selectivity to 1,2-PDO was clearly a maximum for a pressure of 14 bar for both catalysts.
3. Increasing the pressure improves the selectivity to 1,2-PDO because the rate of reaction (2) is increased. Then AOL selectivity decreases.
4. At 20 bar the selectivity to 1,2-PDO reaches a value near 95% for both catalysts. The selectivity to AOL is almost negligible. The selectivity to 1,3-PDO has a value of about 4% at the highest pressure tests, for both catalysts. An alternative reaction path is clearly favored (reactions (5) and (6), Fig. 2).

If the pressure effect is analyzed with the aid of Equation (21) it can be inferred that when the pressure is increased the selectivity to 1,2-PDO is increased. The regime would not be affected by this change in pressure.

If the catalyst particle size is increased the regime is not altered. If the particle size is decreased the regime can be changed to control by intrapellet diffusion or chemical control.

Catalysts activity comparison

A comparison is indeed difficult due to the mass transfer restrictions detected. However on an approximate basis points of similar conversion, far from 99%+, can be compared if gas–liquid resistance is assumed to be constant. Or points with similar W/F. These data points (taken from the data set of Fig. 10) could be: (i) CA catalyst, 35% conversion, W/F = 1282 g min mol^{-1}, r = 0.27 mmol g^{-1} min^{-1}; (ii) CA catalyst, 21.8% conversion, W/F = 855 g min mol^{-1}, r = 0.26 mmol g^{-1} min^{-1}; (iii) CC catalyst, 29% conversion, W/F = 855 g min mol^{-1}, r = 0.34 mmol mmol g^{-1} min^{-1}. The CC catalyst is the most active, yielding a 26–30% higher rate of conversion per unit mass than the CA catalyst. The bulk density of CC is also higher than that of CA (2.1 and 1.63 g cm^{-3}, respectively). Hence CC is also more active per unit reactor volume.

CONCLUSIONS

A network of possible reactions was studied in order to determine their thermodynamic feasibility. Most relevant reactions were found to be irreversible or reversible, however only a subset was found to be occurring according to compositional data from chromatography.

Another study of the phase equilibrium of the feed and the fluodynamic conditions inside the packed bed reactor indicated that the reaction system had three phases, gas (hydrogen, Gly and water), liquid (Gly, water, dissolved hydrogen) and solid (catalyst), and that the flow regime is 'trickling'. Theoretical estimations indicated that the catalyst particles are isothermal and that there exists a significant mass transfer resistance for the movement of hydrogen from the gas to the liquid phase.

The catalytic test results indicated that hydrogenations were faster than dehydrations. The latter would be the slow rate-determining step of the reaction network taking place on the catalyst surface sites.

Copper over alumina and copper chromite catalysts had very different physical and chemical properties (specific surface area, pore volume, pore size distribution, crystal phase, copper content, acidity). However they had similar surface active Cu sites, as determined by XPS. The catalytic activity would be associated to surface Cu^0 sites.

The reaction tests yielded similar results for both catalysts. This was not expected and prompted an analysis of the operating mass transfer phenomena. A comparison of all resistances, diffusion–reaction, gas–liquid, and solid–liquid, indicated that gas–liquid resistance dominated the conversion of Gly in the trickle-bed reactor. Moreover, it was found that the observed conversion rate was approximately equal to the rate of hydrogen supply from the gas to the liquid phase. In this situation, the rate of conversion of Gly was insensitive to the values of (W/F_A^0) and only depended on the pressure of hydrogen.

A variation of reaction variables was made in order to assess their influence on the catalytic properties. Optimal conditions were found to be 230 °C and 14 bar hydrogen pressure, using 1.9 h^{-1} liquid space velocity. With these conditions 97% selectivity to 1,2-PDO and complete conversion of Gly were obtained.

High temperatures produced a decrease in the selectivity to 1,2-PDO due to the formation of different by-products. With CC mainly 3-HP and 1,3-PDO are produced while with CA mainly minor alcohols (EtOH and MeOH) and AO are to be found. These differences were attributed to the different acidity of the catalysts.

NOTATION

Gly	Glycerol
1,2-PDO	1,2-propanediol
AOL	Acetol
PrAL	Propanal
PrOH	1-Propanol
3-HP	3-Hydroxypropanal
AO	Acetone
MeOH	Methanol
EtOH	Ethanol
1,3-PDO	1,3-propanediol
$\hat{r}$	Average reaction rate per unit mass of catalyst
X_{Gly}	Glycerol conversion
W	Catalyst mass
F^0_{Gly}	Glycerol feed flow rate
R_p, d_p	Particle size (radius and diameter respectively)
CA	Alumina supported Cu catalyst
CC	Copper chromite catalyst
Φ	Weisz-Prater modulus
ρ_p	Catalyst particle density
D_e	Effective diffusivity
D_M	Molecular diffusivity
ε	Porosity
R_{L-S}	Liquid–Solid resistance
R_{G-L}	Gas–Liquid resistance
R_{D-R}	Diffusion–Reaction resistance
ΔH_H	Heat of reaction
C_S	Concentration at the surface
k_e	Effective thermal conductivity
C_L	Concentration in the liquid phase
ξ	Effectiveness factor
k	Kinetic constant
h	Thiele modulus
k_s	Film mass transfer coefficient at the *S-L* interphase
j_D	Adimensional number for mass transfer
$Re_{t,L}$ $Re_{p,L}$	Reynolds number for the liquid phase, related to the tube or the particle
u_L	Liquid velocity
μ_L	Liquid viscosity
ρ_L	Liquid density
H	Henry's equilibrium constant for gas dissolution in the liquid
Q	Flow of molecules per unit interfacial area
a_g	Area per unit volume of the gas–liquid interface
a_c	Area per unit volume of catalyst particle
k_G	Film mass transfer coefficient in the *G-L* interphase, gas side
k_L	Film mass transfer coefficient in the *G-L* interphase, liquid side
D_L	Liquid diffusivity
D	Molecular diffusivity in gas or liquid media
N_{Gly}	Moles of glycerol
a_g	Area per unit volume of the gas–liquid interface
C^{eq}_{L,H_2}	Equilibrium concentration of dissolved hydrogen in the liquid phase
$S_{1,2-PDO}$	Selectivity of 1,2-propanediol
R	Constant of ideal gases
P	Pressure
T	Temperature

ACKNOWLEDGEMENTS

We thank Fernanda Mori and María Ana Vicerich for their helpful technical assistance. We also thank ANPCyT for financing the purchase of a SPECS multitechnique analysis instrument (PME8-2003 Grant) that was used in this work.

REFERENCES

1 Seretis A and Tsiakaras P, Hydrogenolysis of glycerol to propylene glycol by in situ produced hydrogen from aqueous phase reforming of glycerol over SiO_2-Al_2O_3 supported nickel catalyst. *Fuel Process Technol* **142**:135–146 (2016).

2 Nakagawa Y, Ning X, Amada Y and Tomishige K, Solid acid co-catalyst for the hydrogenolysis of glycerol to 1,3-propanediol over Ir-ReO_x/SiO_2. *Appl Catal A* **433–434**:128–134 (2012).

3 Kwak BK, Park DS, Yun YS and Yi J, Preparation and characterization of nanocrystalline $CuAl_2O_4$ spinel catalysts by sol–gel method for the hydrogenolysis of glycerol. *Catal Commun* **24**:90–95 (2012).

4 Deng C, Leng L, Duan X, Zhou J, Zhou X and Yuan W, Support effect on the bimetallic structure of Ir–Re catalysts and their performances in glycerol hydrogenolysis. *J Mol Catal A-Chem* **410**:81–88 (2015).
5 Mallesham B, Sudarsanam P, Reddy BVS and Reddy BM, Development of cerium promoted copper–magnesium catalysts for biomass valorization: selective hydrogenolysis of bioglycerol. *Appl Catal B* **181**:47–57 (2016).
6 Vanama P, Kumar A, Ginjupalli S and Komandur VRC, Vapor-phase hydrogenolysis of glycerol over nanostructured Ru/MCM-41 catalysts. *Catal Today* **250**:226–238 (2015).
7 Guo L, Zhou J, Mao J, Guo X and Zhang S, Supported Cu catalysts for the selective hydrogenolysis of glycerol to propanediols. *Appl Catal A* **367**:93–98 (2009).
8 Chiu C, *Catalytic conversion of glycerol to propylene glycol: synthesis and technology assessment*. Doctoral Thesis, University of Missouri-Columbia (2006).
9 Feng Y, Liu C, Kang Y, Zhou X, Liu L, Deng J *et al.*, Selective hydrogenolysis of glycerol to 1,2-propanediol catalyzed by supported bimetallic PdCu-KF/γ-Al_2O_3. *Chem Eng J* **281**:96–101 (2015).
10 Soares A, Perez G and Passos FB, Alumina supported bimetallic Pt–Fe catalysts applied to glycerol hydrogenolysis and aqueous phase reforming. *Appl Catal B - Environ* **185**:77–87 (2016).
11 Deng C, Leng L, Zhou J, Zhou X and Yuan W, Effects of pretreatment temperature on bimetallic Ir-Re catalysts for glycerol hydrogenolysis. *Chinese J Catal* **36**:1750–1758 (2015).
12 Sun D, Yamada Y and Sato S, Effect of Ag loading on Cu/Al2O3 catalyst in the production of 1,2-propanediol from glycerol. *Appl Catal A* **475**:63–68 (2014).
13 Mota CJA, Goncalves VLC, Mellizo JE, Rocco AM, Fadigas JC and Gambetta R, Green propene through the selective hydrogenolysis of glycerol oversupported iron-molybdenum catalyst: the original history. *J Mol Catal A* **422**:158–164 (2015).
14 Liu L and Ye XP, Simultaneous production of lactic acid and propylene glycol from glycerol using solid catalysts without external hydrogen. *Fuel Process Technol* **137**:55–65 (2015).
15 Seretis A and Tsiakaras P, Aqueous phase reforming (APR) of glycerol over platinum supported on Al_2O_3 catalyst. *Renew Energy* **85**:1116–1126 (2016).
16 Jiang T, Huai Q, Geng T, Ying W, Xiao T and Cao F, Catalytic performance of Pd-Ni bimetallic catalyst for glycerol hydrogenolysis. *Biomass Bioenergy* **78**:71–79 (2015).
17 Zhou Z, Li X, Zeng T, Hong W, Cheng Z and Yuan W, Kinetics of hydrogenolysis of glycerol to propylene glycol over Cu-ZnO-Al_2O_3 catalysts. *Chinese J Chem Eng* **18**:384–390 (2010).
18 Zheng L, Xia S and Hou Z, Hydrogenolysis of glycerol over Cu-substituted hydrocalumite mediated catalysts. *Appl Clay Sci* **118**:68–73 (2015).
19 Zhu S, Gao X, Zhu Y, Fan W, Wang J and Li Y, A highly efficient and robust Cu/SiO_2 catalyst prepared by the ammonia evaporation hydrothermal method for glycerol hydrogenolysis to 1,2-propanediol. *Catal Sci Technol* **5**:1169–1180 (2015).
20 Zhu S, Gao X, Zhu X and Li Y, Tailored mesoporous copper/ceria catalysts for the selective hydrogenolysis of biomass-derived glycerol and sugar alcohols. *Green Chem* **18**:782–791 (2016).
21 Cui F, Chen J, Xia C, Kang H, Zhang X and Tong J, Method for producing 1,2-propylene glycol using bio-based glycerol. US Patent 7586016 (2009).
22 Franke O and Stankowiak A, Process for preparing 1,2-propanediol by hydrogenolysis of glycerol. US Patent 7812200 (2010).
23 Stankowiak A and Franke O, Method for preparing 1,2-propanediol by hydrogenolysis of glycerol. US Patent 7868212 (2011).
24 Bloom P, Hydrogenolysis of glycerol and products produced therefrom. US Patent 8153847 (2012).
25 Checa M, Marinas A, Marinas JM and Urbano FJ, Deactivation study of supported Pt catalyst on glycerol hydrogenolysis. *Appl Catal A* **507**:34–43 (2015).
26 Wu Z, Mao Y, Song M, Yin X and Zhang M, Cu/boehmite: a highly active catalyst for hydrogenolysis of glycerol to 1,2-propanediol. *Catal Commun* **32**:52–57 (2013).
27 Wang C, Jiang H, Chen C, Chen R and Xing W, Solvent effect on hydrogenolysis of glycerol to 1,2-propanediol over Cu–ZnO catalyst. *Chem Eng J* **264**:344–350 (2015).
28 Mane RB, Ghalwadkar AA, Hengne AM, Suryawanshi YR and Rode CV, Role of promoters in copper chromite catalysts for hydrogenolysis of glycerol. *Catal Today* **164**:447–450 (2011).
29 Vicerich MA, Benitez VM, Especel C, Epron F and Pieck CL, Influence of iridium content on the behavior of Pt-Ir/Al2O3 and Pt-Ir/TiO2 catalysts for selective ring opening of naphthenes. *Appl Catal A* **453**:167–174 (2013).
30 Yuan Z, Wang J, Wang L, Xie W, Chen P, Hou Z *et al.*, Biodiesel derived glycerol hydrogenolysis to 1,2-propanediol on Cu/MgO catalysts. *Bioresource Technol* **101**:7088–7092 (2010).
31 Corma A, Huber GW, Sauvanaud L and O'Connor P, Biomass to chemicals: catalytic conversion of glycerol/water mixtures into acrolein, reaction network. *J Catal* **257**:163–171 (2008).
32 NIST Chemistry Webbook Database, National Institute of Standards and Technology, USA.
33 Physical Properties Table, Mc Graw Hill Higher Education (2005).
34 Tong C, Blanco M, Goddard III WA and Seinfeld JH, Secondary organic aerosol formation by heterogeneous reactions of aldehydes and ketones: a quantum mechanical study. *Environ Sci Technol* **40**:2333–2338 (2006).
35 Cheméo C, *Fluid Phase Equilibria*, Chemical Properties and Databases, Céondo GmBh, Germany (2017).
36 Joback KG, *Unified approach to physical property estimation using multivariate statistical techniques*. MS Thesis, MIT, Cambridge, MA (1984).
37 Lewars E and Liebman JF, What are the enthalpy of formation and the stabilization energy of acrolein. *Struct Chem* **24**:741–744 (2013).
38 Pala Rosas I, Contreras JL, Salmones J, Tapia C, Zeifert B, Navarrete J *et al.*, Catalytic dehydration of glycerol to acrolein over a catalyst of Pd/LaY zeolite and comparison with the chemical equilibrium. *Catal* **7**:73–102 (2017).
39 Huang L, Zhu YL, Zheng HY, Li YW and Zeng ZY, Continuous production of 1,2-propanediol by the selective hydrogenolysis of solvent-free glycerol under mild conditions. *Chem Technol Biotechnol* **83**:1670–1675 (2008).
40 Akiyama M, Sato S, Takahashi R, Inui K and Yokota M, Dehydration–hydrogenation of glycerol into 1,2-propanediol at ambient hydrogen pressure. *Appl Catal A* **371**:60–66 (2009).
41 Wang J, Wang W, Huo S, Lee M and Kollman PA, Solvation model based on weighted solvent accessible surface area. *J Phys Chem B* **105**:5055–5067 (2001).
42 Charpentier JC and Favier M, Some liquid holdup experimental data in trickle bed reactors for foaming and nonfoaming hydrocarbons. *AIChE J* **21**:1213–1218 (1975).
43 Tosun G, A study of cocurrent downflow of nonfoaming gas–liquid systems in a packed bed. 1. Flow regimes: search for a generalized flow map. *Ind Eng Chem Process Des Dev* **23**:29–35 (1984).
44 Vila F, López Granados M, Ojeda M, Fierro JLG and Mariscal R, Glycerol hydrogenolysis to 1,2-propanediol with Cu/γ-Al_2O_3: effect of the activation process. *Catal Today* **187**:122–128 (2012).
45 Durán-Martín D, Ojeda M, López Granados M, Fierro JLG and Mariscal R, Stability and regeneration of Cu–ZrO_2 catalysts used in glycerol hydrogenolysis to 1,2-propanediol. *Catal Today* **210**:98–105 (2013).
46 Liang C, Li X, Qu Z, Tade M and Liu S, The role of copper species on Cu/Al_2O_3 catalysts for NH_3–SCO reaction. *Appl Surf Sci* **258**:3738–3743 (2013).
47 Larsson PO and Andersson A, Oxides of copper, ceria promoted copper, manganese and copper manganese on Al_2O_3 for the combustion of CO, ethyl acetate and ethanol. *Appl Catal B* **24**:175-192 (2000).
48 Villaverde MM, Bertero NM, Garetto TF and Marchi AJ, Selective liquid-phase hydrogenation of furfural to furfuryl alcohol over Cu-based catalysts. *Catal Today* **213**:87–92 (2013).
49 McIntyre NS and Cook MG, X-ray photoelectron studies on some oxides and hydroxides of cobalt, nickel, and copper. *Anal Chem* **47**:2208–2213 (1975).
50 Busto M, Benitez VM, Vera CR, Grau JM and Yori JC, Pt-Pd/WO_3-ZrO_2 catalysts for isomerization-cracking of long paraffins. *Appl Catal A* **347**:117–125 (2008).
51 Sun D, Yamada Y and Sato S, Efficient production of propylene in the catalytic conversion of glycerol. *Appl Catal B* **174–175**:13–20 (2015).
52 Li Z, Zuo M, Jiang Y, Tang X, Zeng X, Sun Y *et al.*, Stable and efficient CuCr catalyst for the solvent-free hydrogenation of biomass derived ethyl levulinate to c-valerolactone as potential biofuel candidate. *Fuel* **175**:232–239 (2016).
53 Akiyama M, Sato S, Takahashi R, Inui K and Yokota M, Dehydration–hydrogenation of glycerol into 1,2-propanediol at ambient hydrogen pressure. *Appl Catal A* **371**:60–66 (2009).
54 Poling BE, Prausnitz JM and O'Connell JP, *The Properties of Gases and Liquids*, 5th edn. McGraw-Hill, New York, NY (2001).

55 Miner CS and Dalton NN, *Glycerol, American Chemical Society Monograph*. Reinhold Publishing Corp, pp. 1–17 (1953).
56 Drucker E and Moles E, Gaslöslichkeit in wBsseringen Lösungen von Glycerin und Isobuttersa'ure. *Z Physik Chem* **75**:405–436 (1911).
57 D'Angelo JVH and Francesconi AZ, Gas–liquid solubility of hydrogen in n-alcohols ($1 \leq n \leq 4$) at pressures from 3.6 MPa to 10 MPa and temperatures from 298.15 K to 525.15 K. *J Chem Eng Data* **46**:671–674 (2001).
58 Breman BB, Beenackers AACM, Rietjens EWJ and Stege RJH, Gas–liquid solubilities of carbon monoxide, carbon dioxide, hydrogen, water, 1-alcohols ($1 \leq n \leq 6$), and n-paraffins ($2 \leq n \leq 6$) in hexadecane, octacosane, hexadecanol, phenanthrene, and tetraethylene glycol at pressures up to 5.5 MPa and temperatures from 293 to 553 K. *J Chem Eng Data* **39**:647–666 (1994).
59 Marrero TR and Mason EA, Gaseous diffusion coefficients. *J Phys Chem Ref Data* **1**:1–118 (1972).
60 Cussler EL, Diffusion: Mass Transfer in Fluid Systems*, 2nd edn*. Cambridge University Press, New York, NY (1997).
61 Goto S, Levec K and Smith JM, Mass transfer in packed beds with two phase flow. *Ind Eng Chem Process Des Dev* **14**:473–478 (1975).
62 Herskowitz M and Smith JM, Trickle-bed reactors: a review. *AIChE J* **29**:1–18 (1983).
63 Turek W and Lange R, Mass transfer in trickle-bed reactors at low Reynolds number. *Chem Eng Sci* **36:**569–579 (1981).
64 Metaxas K and Papayannakos N, Gas–liquid mass transfer in a bench-scale trickle bed reactor used for benzene hydrogenation. *Chem Eng Technol* **31**:1410–1417 (2008).
65 Prater CD, The temperature produced by heat of reaction in the interior of porous particles. *Chem Eng Sci* **8**:284–286 (1958).
66 Li KT, Wang CH and Wang HC, Hydrogenolysis of glycerol to 1,2-propanediol on copper core-porous silica shell-nanoparticles. *J Taiwan In st Chem Eng* **52**:79–84 (2015).
67 Huang L, Zhu Y, Zheng H, Ding G and Li Y, Direct conversion of glycerol into 1,3-propanediol over Cu-$H_4SiW_{12}O_{40}/SiO_2$ in vapor phase. *Catal Lett* **131**:312–320 (2009).

